Compositional dependence of the apatite formation ability of Ti–Zr alloys designed for hard tissue reconstruction

Toshiki Miyazaki[a], Tomoya Hosokawa[a], Ken'ichi Yokoyama[b], Takanobu Shiraishi[c]

[a]Graduate School of Life Science and System Engineering, Kyushu Institute of Technology, Kitakyushu, Japan

[b]Department of Materials Science and Engineering, Kyushu Institute of Technology, Kitakyushu, Japan

[c]Graduate School of Biomedical Sciences, Nagasaki University, Nagasaki, Japan

Corresponding author: Toshiki Miyazaki

Graduate School of Life Science and Systems Engineering, Kyushu Institute of Technology, 2-4, Hibikino, Wakamatsu-ku, Kitakyushu 808-0196, Japan

Tel./Fax: +81-93-695-6025

E-mail: tmiya@life.kyutech.ac.jp

Abstract

Ti–Zr alloys are expected to be novel biomaterials with low stress shielding owing to their lower Young's moduli than pure Ti. The drawback of metallic biomaterials is that their bone-bonding abilities are relatively low. NaOH and heat treatments have been performed to provide Ti–50Zr with apatite-forming ability in the body environment, which is essential for bone bonding. However, the systematic compositional dependence of apatite formation has not been revealed. In the present study, NaOH treatment of Ti–Zr alloys with various compositions and bone-bonding abilities was assessed in vitro by apatite formation in simulated body fluid (SBF). The corrosion current density in NaOH aqueous solution and the amount of Na incorporated into the surface tended to decrease with increasing Zr content. The apatite-forming ability of the treated alloy significantly decreased when the Zr content was ≥60 atom%. This phenomenon is attributed to the (1) low OH content on the surface, (2) low Na incorporation into the treated alloy surface, which enhances apatite formation, and (3) low ability of P adsorption to the Ti–Zr alloy in SBF following Ca adsorption to trigger apatite nucleation. Although the adhesion of the titanate/zirconate layer formed on the surfaces

to the substrates increased as Zr content increased, the adhesion between the apatite and the substrate was still low.

Keywords: Ti–Zr alloy, NaOH treatment, Apatite, Simulated body fluid, Hard tissue reconstruction

Running Heads: Compositional dependence of the apatite formation ability

1. Introduction

Because metallic materials, such as Ti and its alloys, have high mechanical strength and fracture toughness, they are clinically applied to repair hard tissues, such as bone and joints, under high loaded conditions [1]. However, they have the drawback of poor bone-bonding ability leading to low long-term stability of fixation [2]. Formation of bone-like apatite in a body fluid environment is necessary for the material to bond to bone [3]. This type of apatite formation is known to be reproduced even in simulated body fluid (SBF) that mimics the human body fluid composition [4]. Various surface modifications of Ti, such as NaOH treatment [5], hydrogen peroxide treatment [6], anodic oxidation [7], and hydrothermal treatment [8,9], have been proposed to improve the bone-bonding ability of Ti.

Ti–Zr alloys are expected to be novel biomaterials with low stress shielding owing to their lower Young's moduli than pure Ti. It has mechanical strength comparable to commercialized Ti-29Nb-13Ta-4.6Zr alloy with low Young's moduli [10,11]. Also, Ti–Zr binary system gives solid solution at any composition [12], therefore the galvanic corrosion in body environment can be suppressed. Shiraishi *et al.* [13] fabricated Ti–Zr alloys with various compositions and evaluated their mechanical properties, and they found that the Young's modulus decreases to 90 GPa at Ti–60 atom% Zr. It has also been reported that pure Zr [14] and Ti–50 atom% Zr [15,16] subjected to NaOH treatment (and subsequent heat treatment for some metals) shows apatite-forming ability in SBF. However, the systematic compositional dependence of apatite formation has not been reported.

In this study, Ti–Zr alloys with different compositions were treated with NaOH aqueous solution, and their apatite-formation abilities were investigated *in vitro* using SBF. The surface structural changes caused by NaOH treatment were analyzed spectroscopically and electrochemically, and their affect on apatite formation was investigated.

2. Materials and methods

2.1. Specimen preparation

The Ti–Zr alloys, as well as pure Ti and Zr, were prepared by the arc-melting method. NaOH and the reagents used to prepare SBF were purchased from Nacalai

Tesque Inc. (Kyoto, Japan). NH_4Cl, $ZnCl_2$, NH_3, and HNO_3 aqueous solutions were purchased from FUJIFILM Wako Pure Chemical Co. (Osaka, Japan).

The alloy substrates with dimensions of 5 mm × 5 mm × 1 mm were polished with #500 SiC paper. Hereafter, the Ti–Zr alloys containing *x* atom% Zr are denoted Ti–*x*Zr (*x* = 20–80). Each substrate was then soaked in 5 mL of 5 M NaOH aqueous solution and shaken in a water bath (H-10, Taitec Co., Saitama, Japan) at 60 °C and 120 strokes/min for 1 day. The substrates were then removed from solution, gently washed with ultrapure water, and dried at 60 °C.

2.2. Soaking in SBF

The treated substrates were soaked in 30 mL of SBF containing 142.0 mM Na^+, 5.0 mM K^+, 2.5 mM Mg^{2+}, 147.8 mM Cl^-, 4.2 mM HCO_3^-, 1.0 mM HPO_4^{2-}, and 0.5 mM SO_4^{2-} at 36.5 °C for various periods. The pH of the solution was buffered at 7.40 by 50 mM tris(hydroxymethyl)aminomethane and an appropriate amount of HCl. The SBF was prepared according to the literature [4]. After soaking, the substrates were removed from the SBF and then subjected to ultrasonic cleaning with ultrapure water for 30 min to remove excess water-soluble salts on their surfaces.

2.3. Characterization

The surface structural changes of the substrates were characterized by scanning electron microscopy (SEM, Model S-3500N, Hitachi Co., Tokyo, Japan), energy dispersive X-ray spectroscopy (EDX, Model EX-400, Horiba Co., Kyoto, Japan), and thin-film X-ray diffraction (TF-XRD, MXP3V, Mac Science Ltd., Yokohama, Japan). In the TF-XRD experiments, CuKα X-ray with voltage and current of 30 kV and 40 mA, respectively, was used and the incident beam was fixed at 1° to the surface of each substrate and the scan rate was $0.02°\cdot s^{-1}$. In EDX, the atomic ratio of each element was calculated from the peak area in the EDX spectrum by using ZAF correction method. Three points were measured for each specimen. Specimens for cross-sectional observation were prepared by embedding in light-curing resin (Technovit 4071, KulZer GmbH, Hanau, Germany), cutting and polishing with #80, #120, #240, #500 and #1000 SiC paper.

Rate of corrosion corresponding to surface oxide formation was evaluated by polarization test. It was performed in 1 M NaOH aqueous solution using a potentiostat (HA-151A, Hokuto Denko Co., Tokyo, Japan) equipped with a saturated calomel electrode as the reference electrode and a Pt electrode as the counter electrode [17]. The specimens were embedded in acrylic resin and the cross-section was abraded with #120, #240, and #500 SiC paper. In the polarization test, the sample was first immersed in 1 M NaOH aqueous solution for 10 min, and the approximate corrosion potential was measured. The specimens were then polarized from the corrosion potential to the anode (+1.5 V) or cathode direction (−1.5 V) at a sweep rate of 20 mV min^{-1}. Measurement was performed once for each specimen.

Surface OH formation by NaOH treatment is reported to govern the apatite formation in body environment [5]. Therefore, the concentration of surface OH groups was determined by formation of a zinc complex [18]. The Zn solution was prepared by mixing 500 mL of 4 M NH_4Cl and 250 mL of 0.4 M $ZnCl_2$, adjusting the pH to 6.9 with 25% NH_3 aqueous solution, and finally adjusting the volume to 1000 mL. Each specimen was soaked in 150 mL of the Zn solution for 5 min and washed with 150 mL of ultrapure water for 10 min. The washing operation was repeated three times. Each specimen was then dried for 1 h and soaked in 100 mL of 2.42 M HNO_3 aqueous solution for 10 min. The Zn concentration in the HNO_3 solution was measured by inductively coupled plasma atomic emission spectroscopy (ICPE-9800, Shimadzu Co., Kyoto, Japan). The surface active OH concentration (C_{OH}) was calculated by the following equation [18]:

$$C_{\mathrm{OH}} = \frac{2C_{\mathrm{Zn}}VA}{S} \qquad (1)$$

where C_{Zn}, V, S, and A, are the Zn concentration in the HNO_3 solution (mM), volume of the HNO_3 solution (L), surface area of the specimen (mm^2), and Avogadro number (6.02×10^{23}), respectively. Measurement was performed three to six times for each specimen.

The adhesive strength of the apatite layer formed on the specimens was measured by peeling-off test regulated in JIS K 5600. An adhesive tape (CT-15105P, NICHIBAN Co., Ltd., Tokyo, Japan) was attached on the specimens and detached. This operation was repeated 5 times.

3. Results

SEM images of the specimen surfaces before and after NaOH treatment are shown in Fig. 1. Before treatment, only polishing scratches were observed in any of the specimens. After NaOH treatment, pure Ti and Ti–20Zr showed a network structure composed of flake-like particles of less than 1 μm in size. When the Zr content was 40 or 50 atom%, formation of a layer without a network structure was observed. Above 50 atom% Zr, no layer formed and polishing scratches were observed, similar to before treatment.

The amounts of OH groups on the specimen surfaces before and after NaOH treatment, which were determined by Zn complex formation method, are shown in Fig. 2. For the untreated specimens, the OH amount was about 1×10^{16} mm^{-2} irrespective of the Zr content. In contrast, the OH amount on the NaOH-treated Ti specimen was about 4×10^{16} mm^{-2} and it tended to decrease with increasing Zr content. The OH amount of Ti–20Zr was lower than that of Ti and Ti–40Zr. Detailed reason is not clear at present. However, judging from the results that Na content is almost the same and morphology of the former was a little different from the latter, difference in OH amount may be attributed to specific surface area. When the Zr content was ≥70 atom%, the OH amount was almost the same as that of the untreated specimens.

The relationship between the Na/(Ti+Zr) ratio on the NaOH-treated specimen surface and the Zr content, which were determined by EDX quantitative analyses, is shown in Figure 3. The Na/(Ti+Zr) ratio was 0.12 for pure Ti. With increasing Zr content, the Na/(Ti+Zr) ratio increased until 40 atom% Zr and then decreased. Na was hardly detected at Zr content ≥80 atom%.

The relationship between the corrosion current density of the specimen in 1 M NaOH aqueous solution and the Zr content is shown in Figure 4. The corrosion current density monotonically decreased with increasing Zr content, indicating that the corrosion resistance against NaOH increased.

The TF-XRD patterns of the untreated and NaOH-treated specimens are shown in Fig. 5. Only the diffraction peaks assigned to the alloys were observed for the untreated specimen. The diffraction angle shifted to lower angle with increasing Zr content. This agrees with the Ti–Zr phase diagram showing an all-proportional solid solution [12]. After NaOH treatment, peaks assigned to crystalline zirconium titanate were only observed for Ti–60Zr and Ti–70Zr.

SEM-EDX profiles of cross-sections of NaOH-treated specimens. in Fig. 6.

Concentration gradient of change Ti and Zr increased with increase in Zr content, suggesting that the thickness of the surface oxide layer is decreased.

SEM images of the specimen surfaces after NaOH treatment and subsequent immersion in SBF for 7 days are shown in Fig. 7. Spherical particles formed on the samples with Zr content ≤50 atom%. In the TF-XRD patterns of the specimens shown in Fig. 8, broad peaks assigned to poorly crystalline apatite (JCPDS#09-0432) are observed at 2θ = 26° and 32° for Zr content ≤50 atom%. This means that the formed spherical particles were poorly crystalline apatite.

The (Ca or P)/(Ti+Zr) molar ratios of the specimen surfaces with Zr content of ≥60 atom% after soaking in SBF for 7 days, where no apatite formed, are shown in Fig. 9. They were determined by EDX quantitative analyses. Both Ca and P were detected for 60 atom% Zr, while only Ca was detected for ≥70 atom% Zr.

Figure 10 shows SEM images of the specimen surfaces after NaOH treatment and subsequent immersion in SBF for 7 days, which were attached and detached with an adhesive tape 5 times. Surface titanate/zirconate layer as well as the apatite particles was peeled-off for pure Ti and 20 atom% Zr, while only the apatite particles for 40 atom% Zr and 50 atom% Zr.

4. Discussion

The thickness of the surface reaction product significantly decreased at high Zr content (>50 atom% Zr). This is attributed to reduction of the reactivity against NaOH aqueous solution. This assumption is supported by the data showing reduction of the corrosion current and OH concentration (see Figs. 2 and 4).

The surface phases on the alloys produced by NaOH treatment significantly varied depending on the Zr content. The surface phases on the alloys predicted from the data in Figs. 2, 3, and 5 are given in Table 1. According to the Pourbaix diagram, $HTiO_3^-$ and $HZrO_3^-$ are stable chemical species around pH 14.7, corresponding to 5 M NaOH, meaning that sodium (hydrogen) titanate/zirconate favorably forms [19]. However, the present result showing no Na incorporation into NaOH-treated Zr is different from that predicted from the Pourbaix diagram (see Fig. 3). It has been reported that although Na is observed on the top surface of Zr treated with 6.1 M NaOH at 50 °C by X-ray photoelectron spectroscopy (XPS), it disappears after Ar^+ sputtering for 6 s [20]. Therefore, Na may exist only on the top surface of the present specimens. However, from the fact that Zr has a significantly lower corrosion rate than Ti in NaOH solution [20], zirconia hydrogel would be the dominant phase. This is consistent with the report by Uchida *et al.* [14], where zirconia hydrogel formed after 20 M NaOH treatment.

When the Zr content exceeded 50 atom%, the apatite-forming ability significantly decreased (see Figs. 7 and 8). From the result that the specimens formed with the zirconium titanate phase did not precipitate apatite, the zirconium titanate phase would not contribute to apatite formation. Ti–OH [21] and Zr–OH [22] groups trigger heterogeneous apatite nucleation in the body environment. Therefore, the decrease in the OH amount shown in Fig. 2 would suppress apatite formation. In addition, for NaOH-treated Ti, Na^+ released from the surface sodium titanate is known to increase the pH of SBF by ion exchange with H_3O^+ and the supersaturation degree with respect to apatite, leading to enhancement of apatite formation [5]. In this study, all the specimens showed pH increase by 0.1 to 0.17 after soaking in SBF for 1 day (Data not shown). In the case of the alloys with high Zr content, judging from the result that Na is hardly incorporated, pH increase would be attributed to another factor such as dissolution of zirconium hydroxide on the surfaces [23]. However, the present results indicate that pH increase do not contribute to the apatite formation at high Zr content.

Adsorption of P was not observed for the alloys that did not form apatite (see Fig. 8). Hanawa and co-workers [24,25] investigated the surface structural changes of the surfaces of pure Ti, pure Zr, and Ti–Zr alloys in Hanks' solution by XPS, and they found that pure Zr and Ti–Zr alloys with high Zr content adsorbed P but not Ca. However, such zirconium phosphate was not detected for the present specimens by EDX or XRD. This may be because analytical method or chemical state of surface zirconia is different. In addition, zirconia hydrogel produced by the sol–gel method is known to have the ability of Ca adsorption [26]. This means that the ion adsorption behavior on the passive oxide film on the metal surface and the sol–gel-derived metal oxide hydrogel is different, and the adsorption behavior on the surfaces of the present alloys is relatively close to the latter. Apatite nucleation on NaOH- and heat-treated Ti in SBF is known to proceed by Ca adsorption followed by P adsorption [27]. It has also been reported that if Ca is adsorbed on zirconia hydrogel in advance, the P adsorption capacity increases [26]. Therefore, the apatite-forming ability may be improved on the alloys with high Zr content by appropriate control of the state of Ca adsorption.

The surface potential is also an important factor that governs the apatite-forming ability. Hashimoto *et al.* [28] investigated apatite formation on Ti metal heat treated in various atmospheres, and they found that a highly negatively (−30 to −15 mV) or positively (10 to 15 mV) charged sample tended to form a large amount of apatite. In contrast, the Ti–Hf alloy formed with hafnium titanate with a highly negative zeta potential of about −40 mV did not form apatite [29]. This means that the surface charge suitable for induction of apatite formation is different depending on the substrate. In future, control of the surface potential should also be investigated.

It was found that the adhesion of the titanate/zirconate layer formed on the surfaces to the substrates increased as Zr content increased. Considering that the concentration gradient becomes gentle as Zr content increases, it is assumed that the stress concentration is suppressed by the formation of the graded structure. However, even in the alloys with high Zr content, the adhesion between the apatite and the substrate was low. This is probably because the alloys with high Zr content had a smooth surface after NaOH treatment as shown in Fig. 1, and had little mechanical locking with the apatite. Kim *et al*. reported that heating at 600°C following NaOH treatment is effective for improving the adhesion of surface titanate layer to Ti substrate [30]. However, in this study, the apatite-forming ability was lost for all the specimens after the heat treatment at 600°C (Data not shown). Also, alpha-beta phase transition may occur around 600 to 800°C [12], which deteriorate mechanical properties of the alloys. It is necessary to pursue optimal heat treatment conditions that maintain the apatite-forming ability.

5. Conclusions

We have found that the apatite-forming ability of NaOH-treated Ti–Zr alloys in SBF is highly dependent on the Zr content. Namely, high Zr content significantly suppresses the apatite-forming ability. This phenomenon is attributed to reduction in the reaction rate in NaOH aqueous solution at high Zr content and the low potential for P to adsorb in SBF. In future, enhancement of the apatite-forming ability of Ti–60Zr is required, because it is has the lowest Young's modulus among the Ti–Zr alloys.

Acknowledgments

The authors thank Ms. Akiko Nomura and Mr. Kazuo Obara of the Institute for Materials Research, Tohoku University, Sendai, Japan for their assistance with sample alloy preparation. We thank Tim Cooper, PhD, from Edanz Group (www.edanzediting.com/ac) for editing a draft of this manuscript.

References

1. Breme J, Biehl V. Metallic Biomaterials. Black J, Hastings G, editors. Handbook of Biomaterial Properties, London: Chapman & Hall; 1998:135-213.
2. Yan WQ, Nakamura T, Kobayashi M, Kim HM, Miyaji F, Kokubo T. Bonding of chemically treated titanium implants to bone. J Biomed Mater Res 1997;37:267-275.
3. Kokubo T, Kim HM, Kawashita M. Novel bioactive materials with different mechanical properties. Biomaterials 2003:24:2161-2175.
4. Cho SB, Kokubo T, Nakanishi K, Soga N, Ohtsuki C, Nakamura T, Kitsugi T,

Yamamuro. Dependence of Apatite Formation on Silica Gel on Its Structure: Effect of Heat Treatment. J Am Ceram Soc 1995;78:1769-1774.

5. Kim HM, Miyaji F, Kokubo T, Nakamura T. Preparation of bioactive Ti and its alloys via simple chemical surface treatment. J Biomed Mater Res 1996;32:409-417.

6. Wang XX, Hayakawa S, Tsuru K, Osaka A. A comparative study of in vitro apatite deposition on heat-, H_2O_2-, and NaOH-treated titanium surfaces. J Biomed Mater Res 2001;54:172-178.

7. Yang BC, Uchida M, Kim HM, Zhang Z, Kokubo T. Preparation of bioactive titanium metal via anodic oxidation treatment. Biomaterials 2004;25:1003–1010.

8. Nakagawa M, Zhang L, Udoh K, Matsuya S, Ishikawa K. Effects of hydrothermal treatment with $CaCl_2$ solution on surface property and cell response of titanium implants. J Mater Sci Mater Med 2005;16:985–991.

9. Kawashita M, Matsui N, Miyazaki T, Kanetaka H. Effect of autoclave and hot water treatments on surface structure and in vitro apatite-forming ability of NaOH- and heat-treated bioactive titanium metal. Mater Trans 2013;54:811–816.

10. Niinomi M. Recent research and development in titanium alloys for biomedical applications and healthcare goods. Sci Tech Adv Mater 2003;4:445–454.

11. Ho WF, Chen WK, Wu SC, Hsu HC. Structure, mechanical properties, and grindability of dental Ti-Zr alloys. J Mater Sci Mater Med 2008;19:3179-3186.

12. Hari Kumar KC, Wollants P, Delacy L. Thermodynamic assessment of the Ti-Zr system and calculation of the Nb-Ti-Zr phase diagram. J Alloys Compd 1994;206:121-127.

13. Shiraishi T, Yubuta K, Shishido T, Shinozaki N. Elastic properties of as-solidified Ti-Zr binary alloys for biomedical applications. Mater Trans 2016;57:1986-1992.

14. Uchida M, Kim HM, Miyaji F, Kokubo T, Nakamura T. Apatite formation on zirconium metal treated with aqueous NaOH. Biomaterials 2002;23:313-317.

15. Chen X, Nouri A, Lin YJ, Hodgson PD, Wen C. Effect of surface roughness of Ti, Zr, and TiZr on apatite precipitation from simulated body fluid. Biotech Bioeng 2008;101:378–387.

16. Chen X, Li Y, Hodgson PD, Wen C. In vitro behavior of human osteoblast-like cells (SaOS2) cultured on surface modified titanium and titanium–zirconium alloy.

Mater Sci Eng C 2011;31:1545-1552.

17. Miyazaki T, Sasaki T, Shirosaki Y, Yokoyama K, Kawashita M. Effect of metallographic structure and machining process on the apatite-forming ability of sodium hydroxide- and heat-treated titanium. Bio-Med Mater Eng 2018;29:109–118.

18. Sakamoto H, Hirohashi Y, Saito H, Doi H, Tsutsumi Y, Suzuki Y, Noda K, Hanawa T. Effect of active hydroxyl groups on the interfacial bond strength of titanium with segmented polyurethane through γ-mercapto propyl trimethoxysilane. Dent Mater J 2008;27:81-92.

19. Pourbaix M. Atlas of Electrochemical Equilibria in Aqueous Solutions. Houston: National Association of Corrosion Engineers; 1974.

20. Motooka T, Yamamoto M. Corrosion behavior of Zr, Ti, Ta and Nb in sodium hydroxide solutions. Zairyo-to-Kankyo 2011;60:394-401 (in Japanese).

21. Li P, Ohtsuki C, Kokubo T, Nakanishi K, Soga N, de Groot K. The role of hydrated silica, titania, and alumina in inducing apatite on implants. J Biomed Mater Res 1994;28:7-15.

22. Uchida M, Kim HM, Kokubo T, Miyaji F, Nakamura T. Bonelike apatite formation induced on zirconia gel in a simulated body fluid and its modified solutions. J Am Ceram Soc 2001;84:2041-2044.

23. Kobayashi T, Sasaki T, Takagi I, Moriyama H. Solubility of zirconium (IV) hydrous oxides, J Nucl Sci Tech 2007;44:90-94.

24. Hanawa T, Okuno O, Hamanaka H. Compositional change in surface of Ti-Zr alloys in artificial bioliquid. J Jpn Inst Metals 1992;56:1168-1173 (in Japanese).

25. Tsutsumi Y, Nishimura D, Doi H, Nomura N, Hanawa T. Difference in surface reactions between titanium and zirconium in Hanks' solution to elucidate mechanism of calcium phosphate formation on titanium using XPS and cathodic polarization. Mater Sci Eng C 2009;29:1702-1708.

26. J. Lin, Y. Zhan, H. Wang, M. Chu, C. Wang, Y. He, X. Wang, Effect of calcium ion on phosphate adsorption onto hydrous zirconium oxide, Chem. Eng. J. 309 (2017) 118-129. DOI: 10.1016/j.cej.2016.10.001

27. Takadama H, Kim HM, Kokubo T, Nakamura T. An X-ray photoelectron spectroscopy study of the process of apatite formation on bioactive titanium metal.

J Biomed Mater Res 2001;55:185-193.

28. Hashimoto M, Ogawa T, Kitaoka S, Muto S, Furuya M, Kanetaka H, Abe M, Yamashita H. Control of surface potential and hydroxyapatite formation on TiO2 scales containing nitrogen-related defects. Acta Mater 2018;155:379-385.

29. Miyazaki T, Sueoka M, Shirosaki Y, Shinozaki N, Shiraishi T. Development of hafnium metal and titanium-hafnium alloys having apatite-forming ability by chemical surface modification. J Biomed Mater Res Part B Appl Biomater 2018;106B:2519–2523.

30. Kim HM, Miyaji F, Kokubo T, Nakamura T. Effect of heat treatment on apatite-forming ability of Ti metal induced by alkali treatment. J Mater Sci Mater Med 1997;8:341–347.

Table 1 Predicted surface phases formed on the alloys by NaOH treatment

Zr content in atom%	Surface phase
0	Sodium titanate hydrogel
20, 40	Sodium titanate/zirconate hydrogel
60	Sodium titanate/zirconate hydrogel, Crystalline $ZrTiO_4$
70	Zirconia/titania hydrogel, Crystalline $ZrTiO_4$
80	Zirconia/titania hydrogel
100	Zirconia hydrogel

Figure captions

Figure 1 SEM images of the specimen surfaces before and after NaOH treatment.

Figure 2 Relationships between the amounts of OH groups on the specimen surfaces before and after NaOH treatment and the Zr content, which were determined by Zn complex formation method (n=3 for untreated sample and n=6 for treated sample).

Figure 3 Relationship between the Na/(Ti+Zr) molar ratio on the NaOH-treated specimen surface and the Zr content, which was determined by EDX quantitative analyses (n=3).

Figure 4 Relationship between the corrosion current density of the specimen in 1 M NaOH aqueous solution and the Zr content (n=1).

Figure 5 TF-XRD patterns of the untreated and NaOH-treated specimens.

Figure 6 SEM-EDX profiles of cross-sections of NaOH-treated specimens.

Figure 7 SEM images of the specimen surfaces after NaOH treatment and subsequent immersion in SBF for 7 days.

Figure 8 TF-XRD patterns of the specimen surfaces after NaOH treatment and subsequent immersion in SBF for 7 days.

Figure 9 (Ca or P)/(Ti+Zr) molar ratios of the specimen surfaces with Zr content of ≥60 atom% after soaking in SBF for 7 days, which were determined by EDX quantitative analyses (n=3).

Figure 10 SEM images of the specimen surfaces after NaOH treatment and subsequent immersion in SBF for 7 days, which were attached and detached with an adhesive tape 5 times.

Fig1

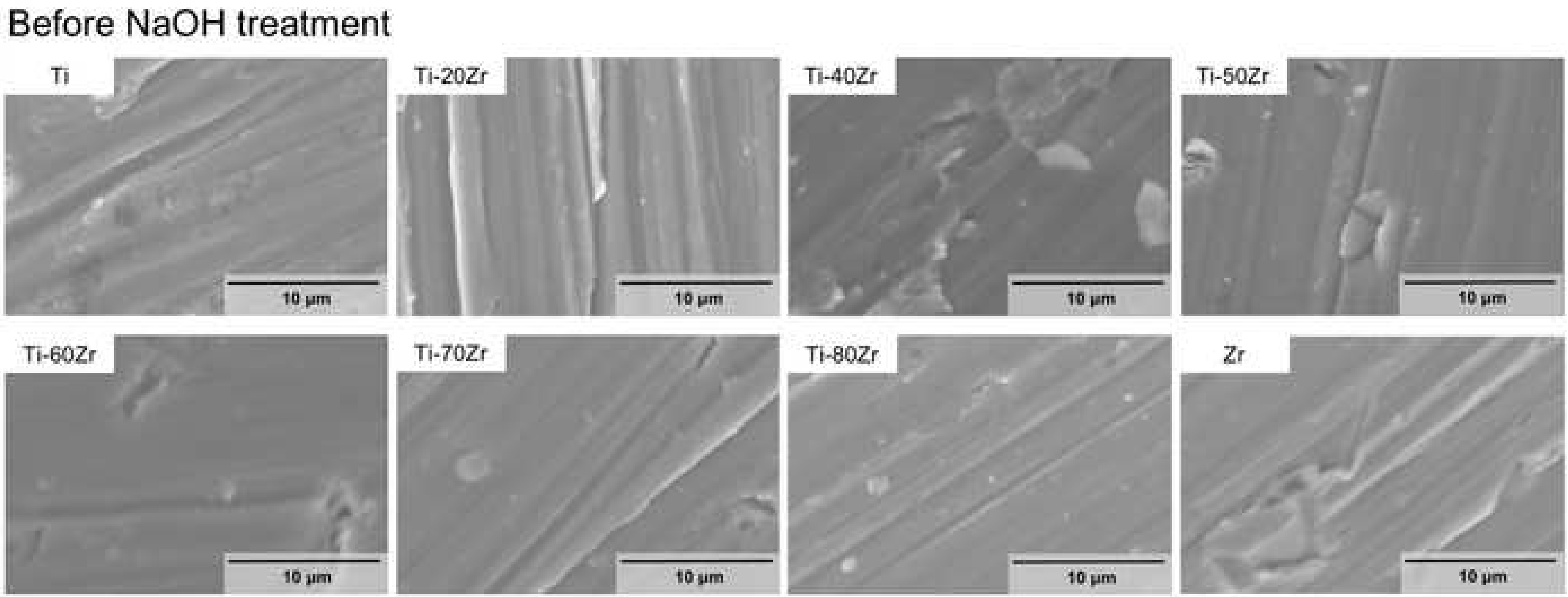
Before NaOH treatment
Ti
Ti-20Zr
Ti-40Zr
Ti-50Zr
Ti-60Zr
Ti-70Zr
Ti-80Zr
Zr
10 µm

Fig. 1

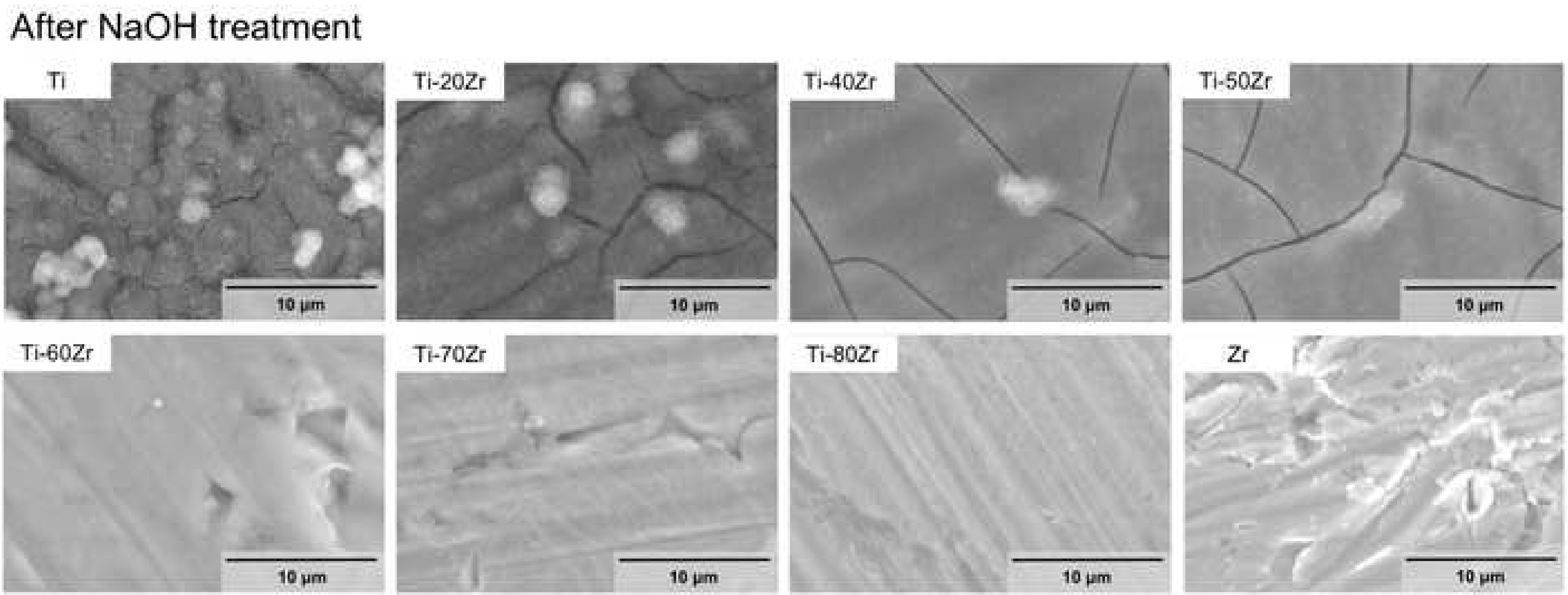

Fig. 1 (Continued)

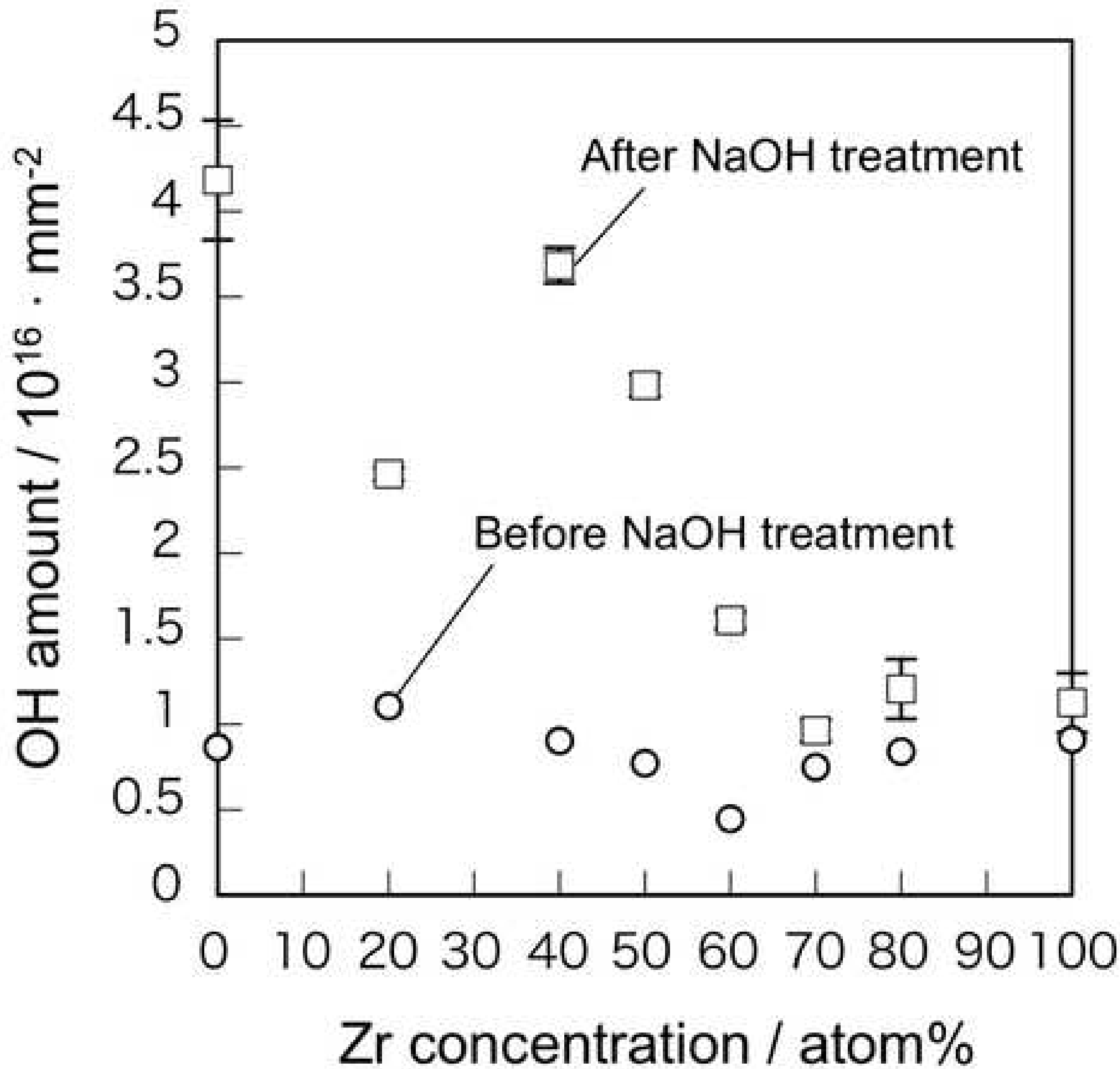

After NaOH treatment
Before NaOH treatment
OH amount / 10^16 · mm^-2
5
4.5
4
3.5
3
2.5
2
1.5
1
0.5
0
0
10
20
30
40
50
60
70
80
90
100
Zr concentration / atom%

Fig. 2

Fig3

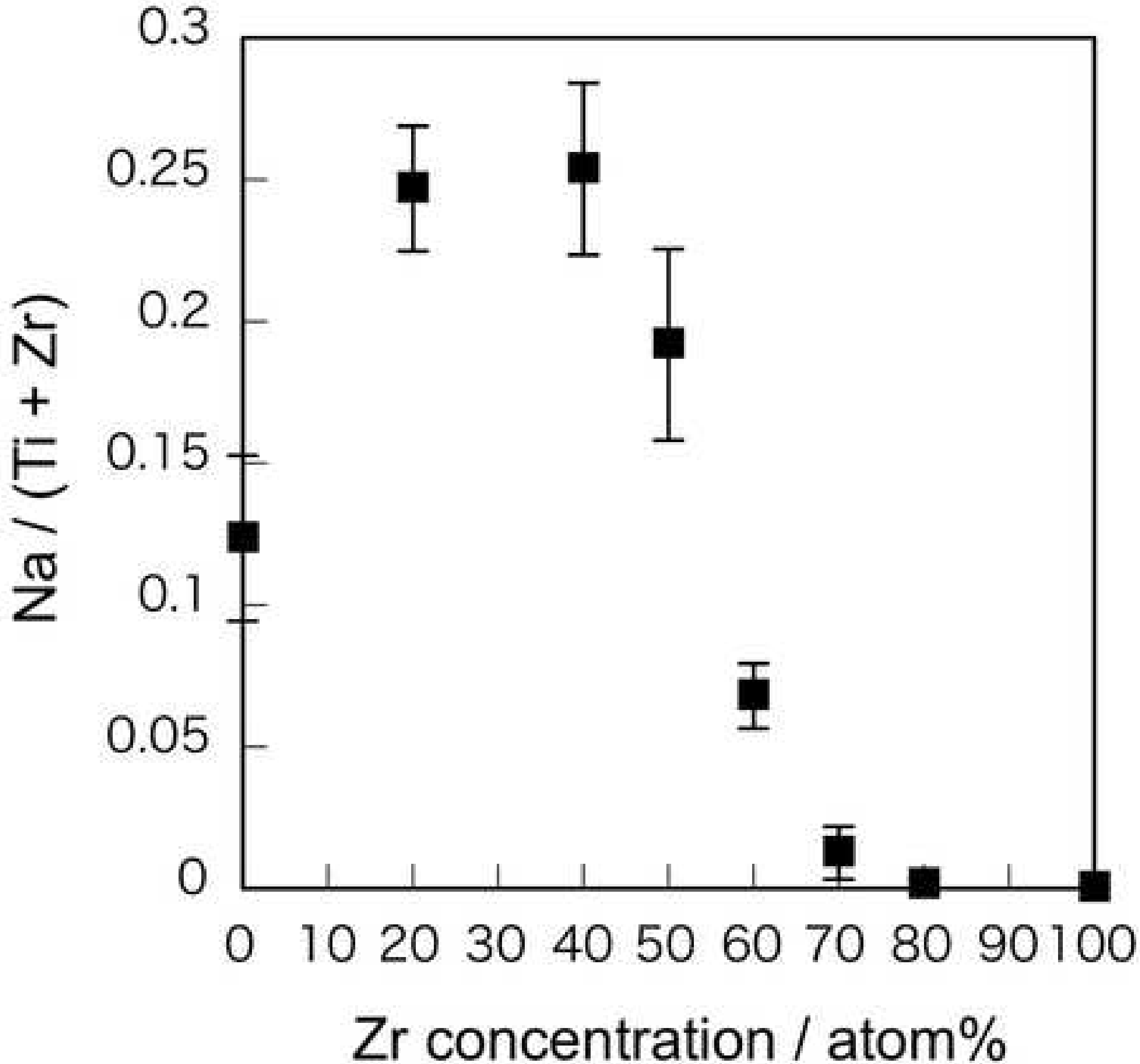
Na / (Ti + Zr)
0.3
0.25
0.2
0.15
0.1
0.05
0
0
10
20
30
40
50
60
70
80
90
100
Zr concentration / atom%

Fig. 3

Fig4 Click here to access/download;Figure;renamed_5cd29.jpg

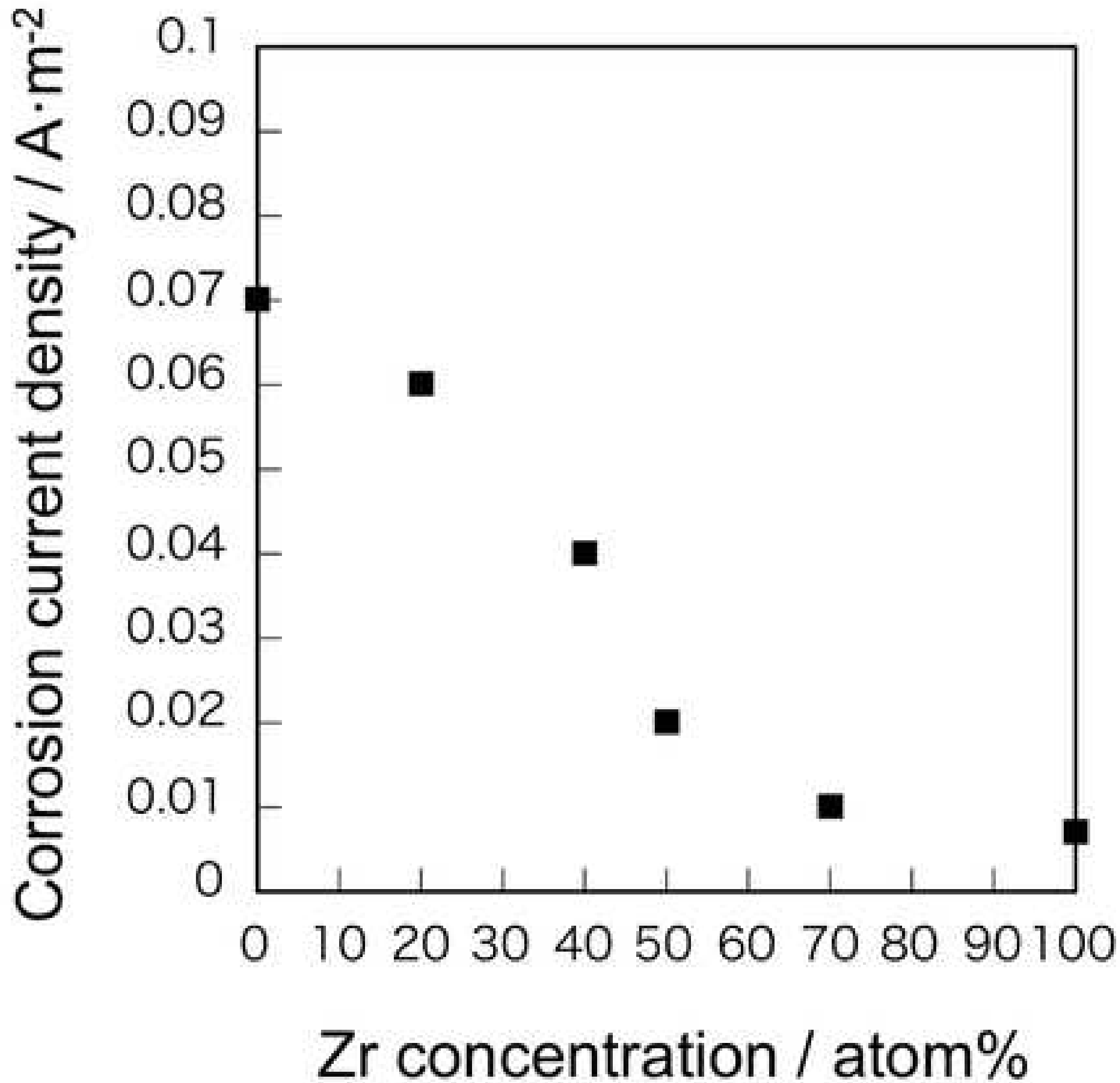

Fig. 4

Fig5

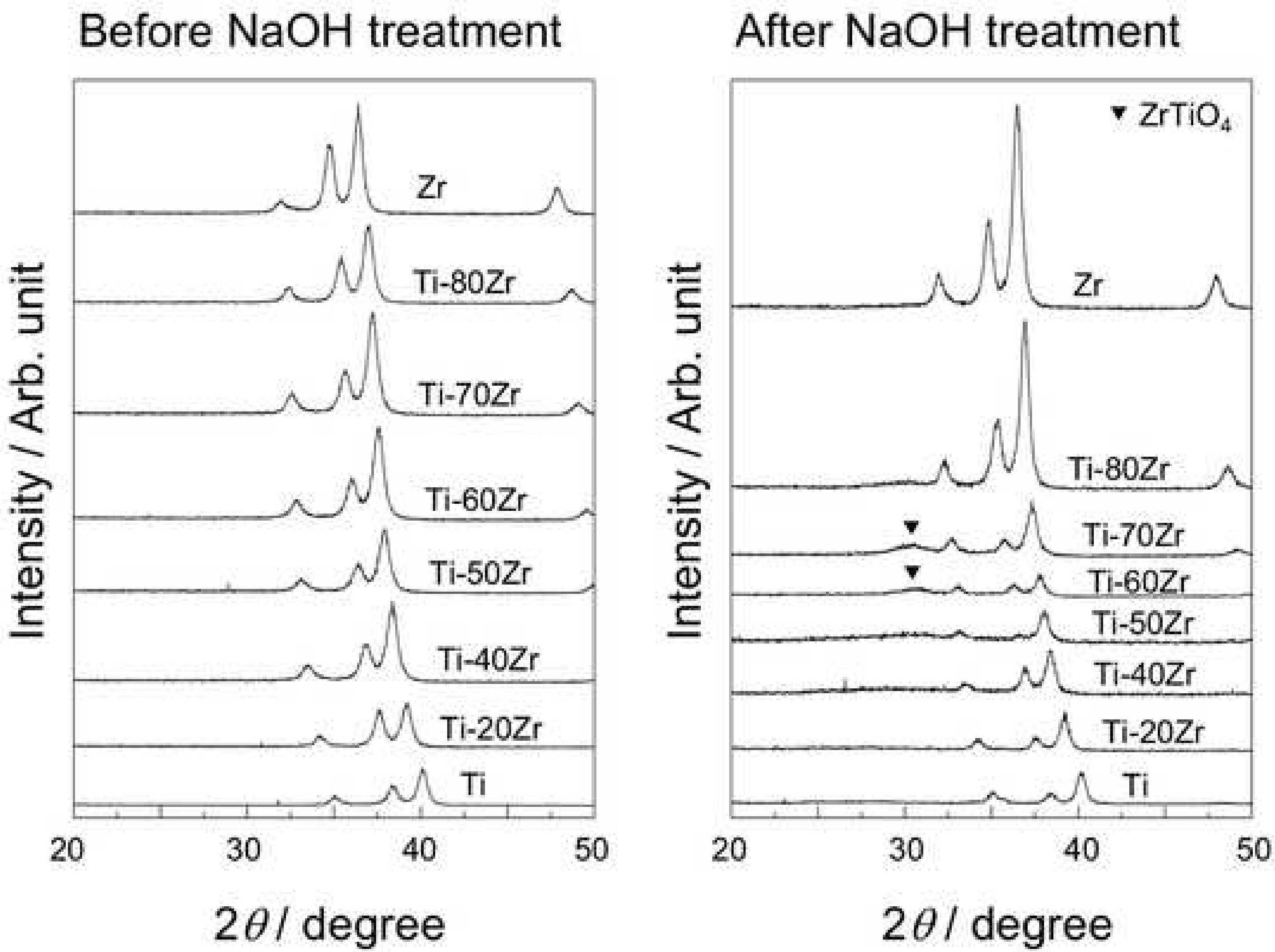
Before NaOH treatment
After NaOH treatment
▼ $ZrTiO_4$
Zr
Ti-80Zr
Ti-70Zr
Ti-60Zr
Ti-50Zr
Ti-40Zr
Ti-20Zr
Ti
Intensity / Arb. unit
20
30
40
50
2θ / degree

Fig. 5

Fig6 Click here to access/download;Figure;renamed_19ad1.jpg

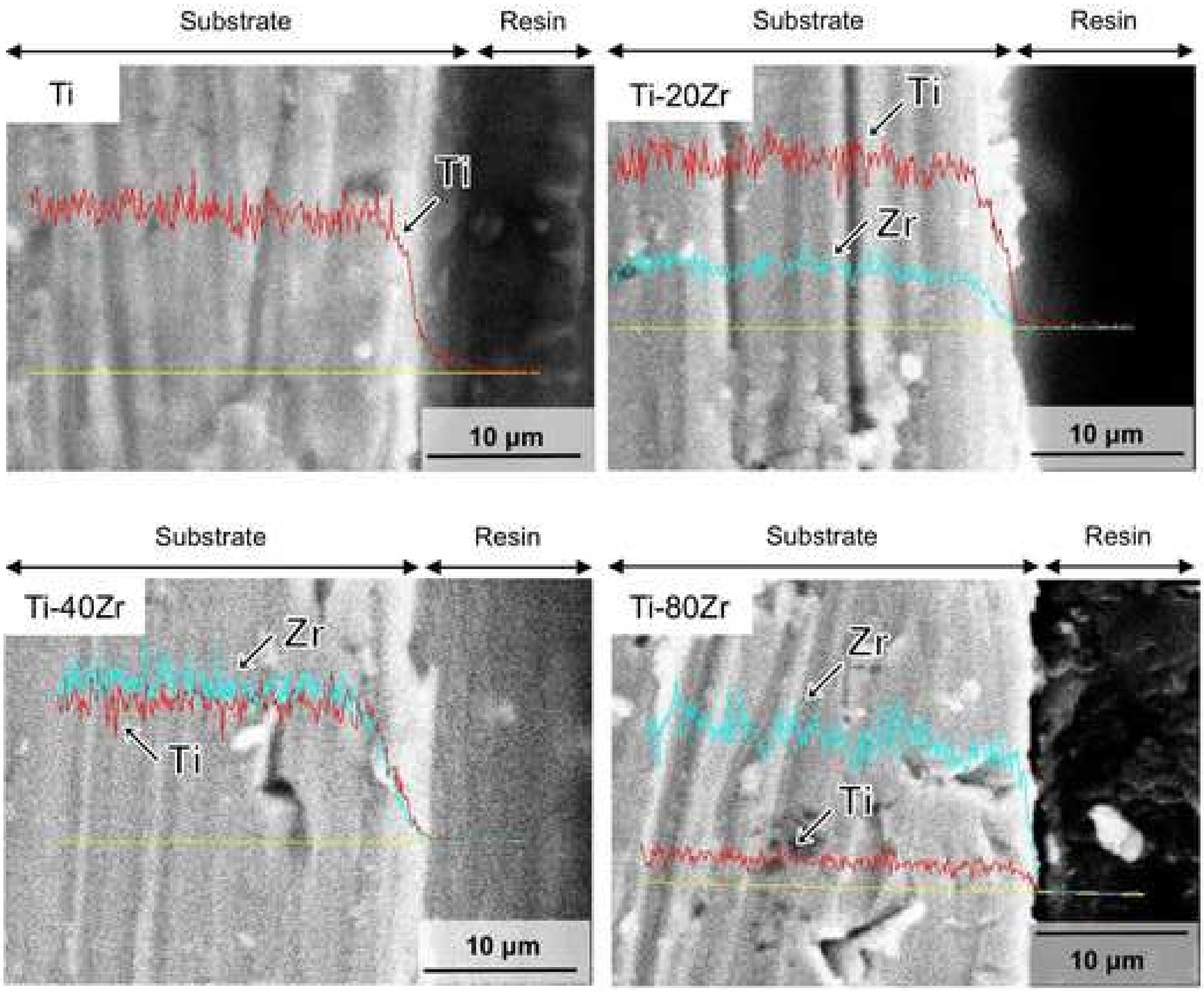

Fig. 6

Fig7

Click here to access/download;Figure;renamed_99669.jpg

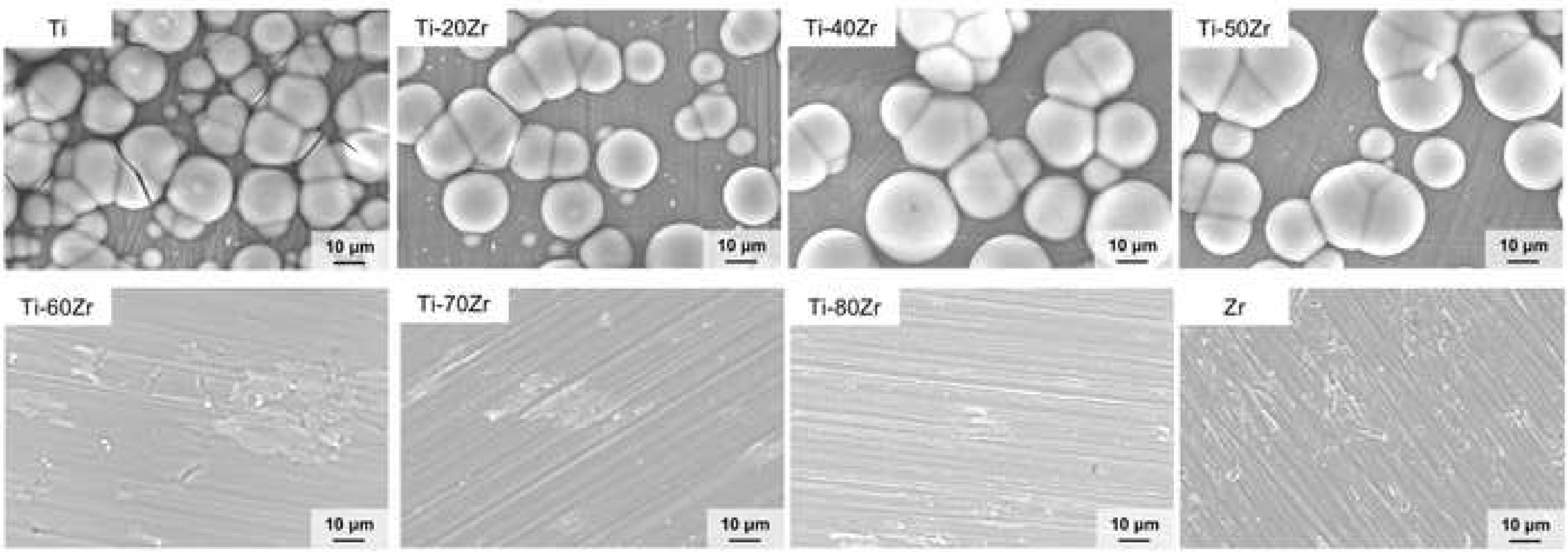

Fig. 7

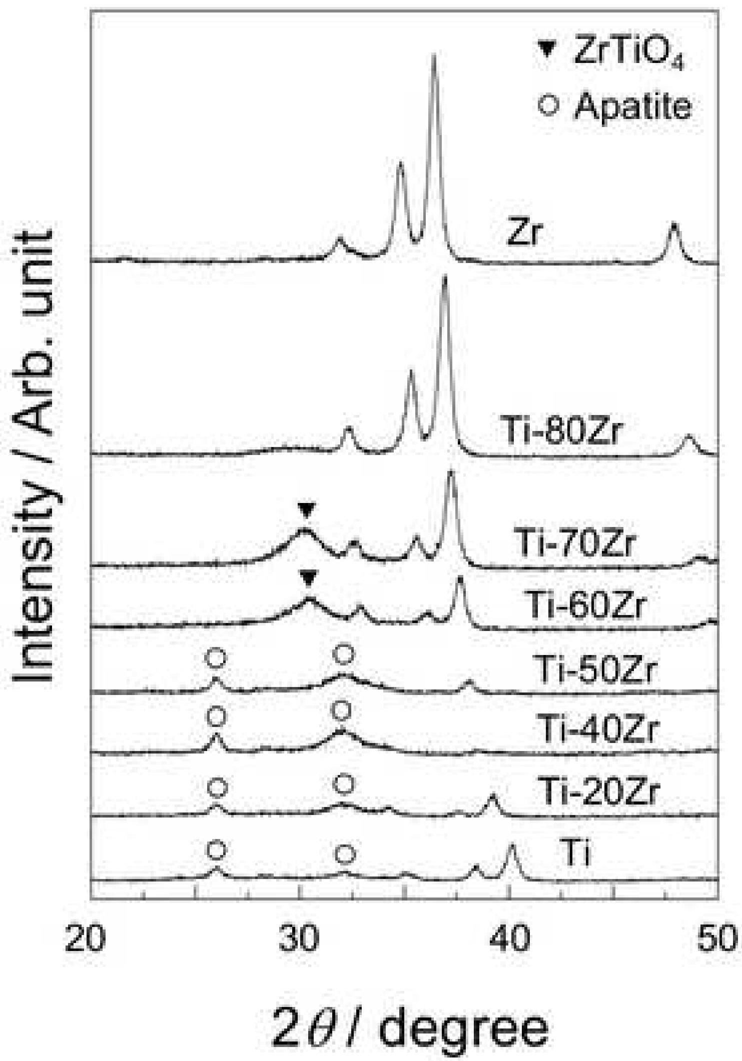

▼ ZrTiO4
○ Apatite
Zr
Ti-80Zr
Ti-70Zr
Ti-60Zr
Ti-50Zr
Ti-40Zr
Ti-20Zr
Ti
Intensity / Arb. unit
20
30
40
50
2θ / degree

Fig. 8

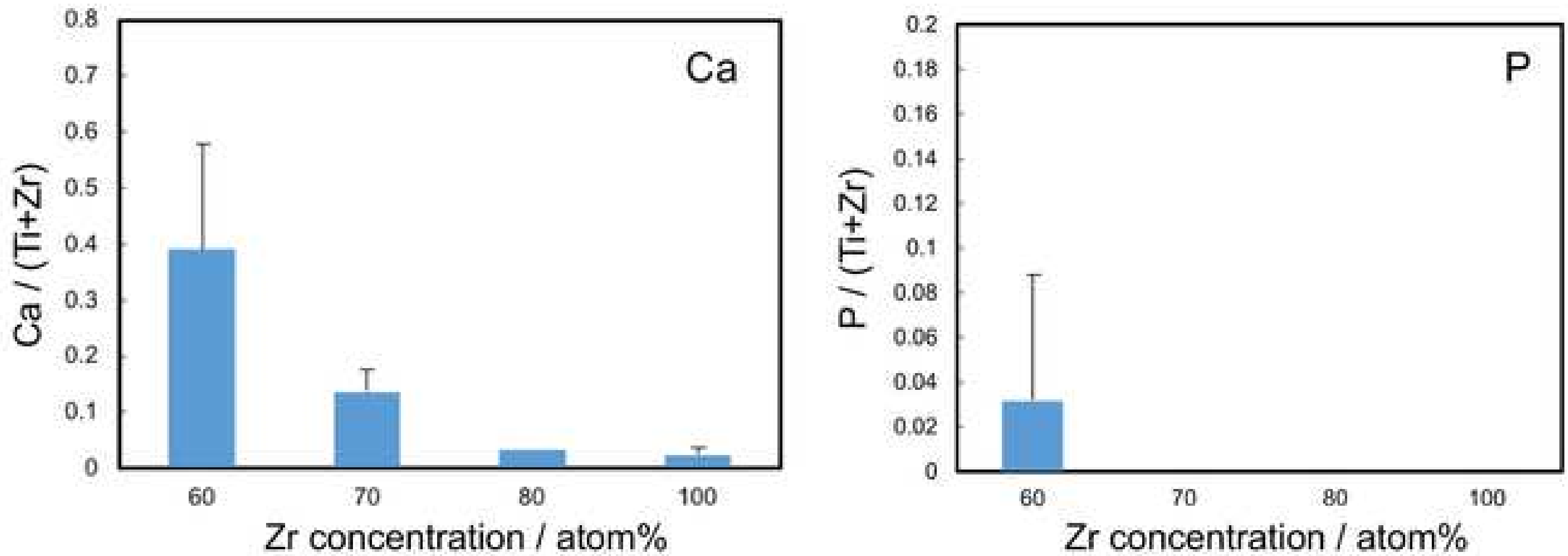
Ca
Ca / (Ti+Zr)
0.8
0.7
0.6
0.5
0.4
0.3
0.2
0.1
0
60
70
80
100
Zr concentration / atom%
P
P / (Ti+Zr)
0.2
0.18
0.16
0.14
0.12
0.1
0.08
0.06
0.04
0.02
0
60
70
80
100
Zr concentration / atom%

Fig. 9

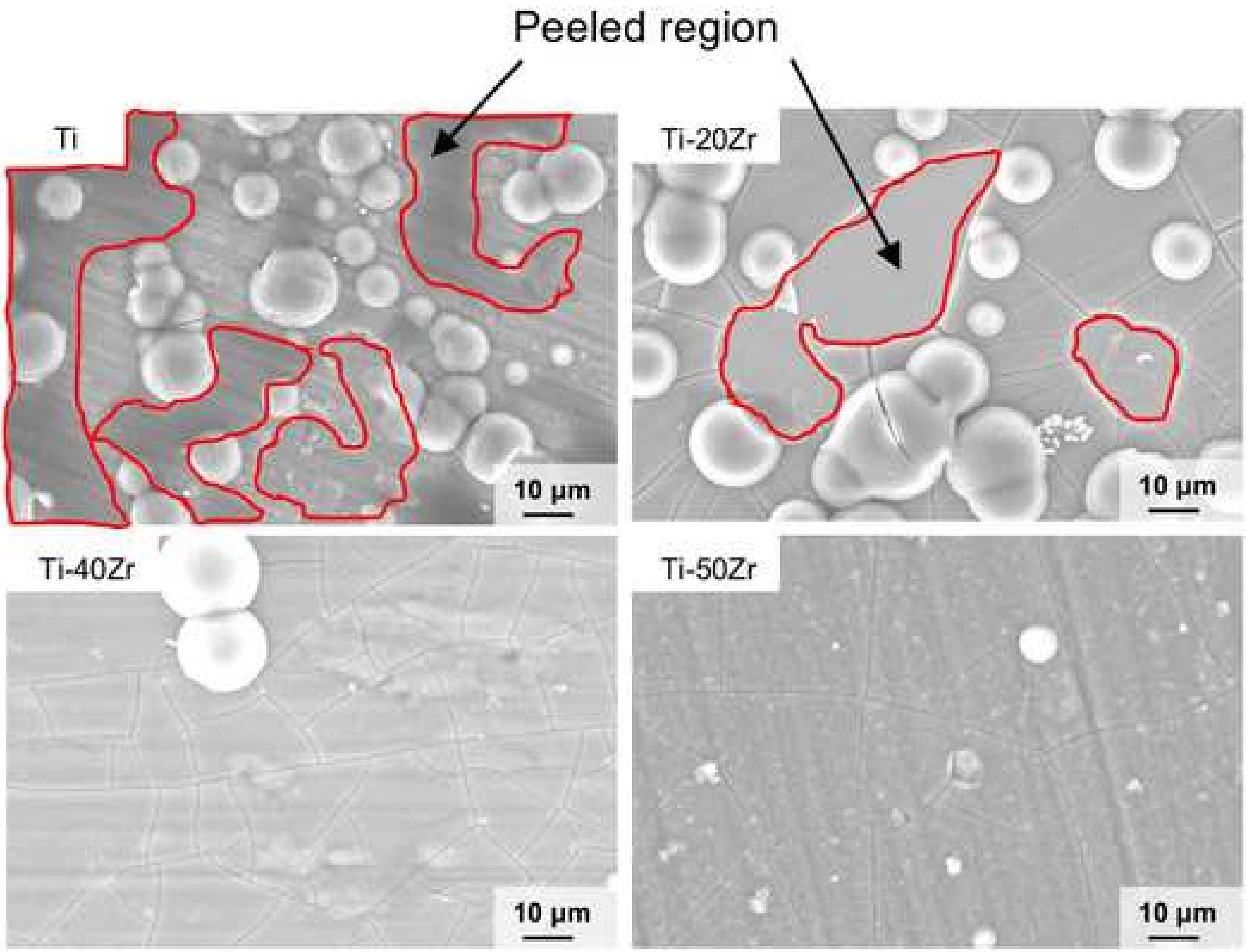

Fig. 10

Graphical Abstract

Click here to access/download;Graphical Abstract;GA.jpg